Science of the Total Environment xxx (xxxx) 136009

Contents lists available at ScienceDirect

Science of the Total Environment

journal homepage: http://ees.elsevier.com

Cr^{3+} substituted Zn-Al layered double hydroxides as UV–Vis light photocatalysts for NO gas removal from the urban environment

Fredy Rodriguez-Rivas [a,b], Adrián Pastor [a], Gustavo de Miguel [c], Manuel Cruz-Yusta [a], Ivana Pavlovic [a], Luis Sánchez [a,*]

[a] Departamento de Química Inorgánica, Instituto Universitario de Nanoquímica IUNAN, Universidad de Córdoba, Campus de Rabanales, E-14014 Córdoba, Spain
[b] Departamento de Química, Facultad de Química y Farmacia, Universidad Nacional Autónoma de Honduras (UNAH), Tegucigalpa, Honduras
[c] Departamento de Química Física y Termodinámica Aplicada, Instituto Universitario de Nanoquímica IUNAN, Universidad de Córdoba, Campus de Rabanales, E-14014 Córdoba, Spain

ARTICLE INFO

Article history:
Received 19 October 2019
Received in revised form 6 December 2019
Accepted 6 December 2019
Available online xxx
Editor: Yifeng Zhang

Keywords
LDH
Zinc
Chromium
Photocatalyst
NO

ABSTRACT

The ZnAl-CO_3, ZnAlCr-CO_3 and ZnCr-CO_3 LDH samples were studied as De-NOx photocatalysts in this work. Samples without Cr and increasing the presence of Cr^{3+} in the LDH framework in the 0.06, 0.15 and 0.3 Cr/Zn ratio were prepared by co-precipitation method, all of them constituted by pure LDH phase. The increase of chromium content in the LDH framework leads to lower crystallinity and higher specific surface area in the samples. Moreover, the CrO_6 octahedron centres expand the photo-activity from UV to Visible light and assist to decrease the recombination rate of the electrons and holes. The favourable textural, optical and electronic properties of Cr-containing LDH samples explain the good NO removal efficiency (55%) and outstanding selectivity (90%) found for the analysed De-NOx process.

1. Introduction

NOx gases (NO and NO_2) are classified as one of the priority air pollutants and they are mainly formed from fossil fuel combustion in automotive and power plants. NOx react with many species and form various toxic products such as nitrate radical, nitrosamines, nitroarenes, etc., which provokes serious negative effects on human health and environment. Human exposure of NOx leads to respiratory and lung problems and even deaths (E.C. Agency, ANNEX 2, Comments and response to comments on CLH proposal on titanium dioxide, 2017; Lee et al., 2014; Sax and Lewis, 2012; Peel et al., 2013). These gases damage the environment because they are involved in phenomena such as acid rain, photochemical smog, and ozone depletion (Boningari and Smirniotis, 2016). However, in urban areas the recommended limit of NOx is often surpassed (Frampton and Greaves, 2009; Williams and Carslaw, 2011; Yamada et al., 2016) and that is the reason of an increasing scientific interest for control and elimination of these air pollutants.

Photocatalysis in the presence of sunlight, atmospheric oxygen and water is one of the most promising technologies for the NO_X abatement (DeNOx process), titanium dioxide being the most studied and applied photocatalyst because of its chemical stability and good UV light response (Balbuena et al., 2018a, 2018b; Ma et al., 2014). However, there is some inconvenience for the use of TiO_2 as semiconductor for this proposal, such as its wide band gap of 3.2 eV which limits its application only to the ultraviolet region of solar irradiation, the low DeNOx selectivity causing the emissions in the atmosphere of the more toxic NO_2 molecules (Balbuena et al., 2018b; Balbuena et al., 2018a), and its potential toxicity when inhaled. Hence, the development of new alternatives to TiO_2 for the DeNOx process is an important scientific topic nowadays.

Layered double hydroxides (LDH) are a class of lamellar solids with the structure similar to those of brucite, where a part of divalent metals is replaced by trivalent ones. This gives rise to an excess of positive charge in the hydroxide sheets which is balanced by intercalating of anions in the interlayer spaces. These compounds of at least two different metal cations, octahedrally-coordinated by hydroxyl groups, have the general formula $[M^{2+}_{1-x}M^{3+}_{x}(OH)_2]^{x+}X^{m-}_{x/m}{\cdot}nH_2O$, where M^{2+} includes divalent cations like Mg^{2+}, Co^{2+}, Ni^{2+}, Cu^{2+}, Zn^{2+} etc., M^{3+} may be Al^{3+}, Fe^{3+}, Cr^{3+} etc., and X might be a huge number of inorganic or organic anions. The atomic ratio between the divalent and trivalent metal which determines the charge density of LDH sheets could vary in a range between 0.20 and 0.33, which could influence on the size-charge fitting of the interlayer anion species (He et al., 2013).

* Corresponding author.
E-mail address: luis-sanchez@uco.es (L. Sánchez)

https://doi.org/10.1016/j.scitotenv.2019.136009
0048-9697/

Their unique properties, wide range of composition variety, ease of preparation and low cost, make these materials suitable for many applications such as catalysts, catalyst supports and precursors (Cavani et al., 1991; Fan et al., 2014), adsorbents (Abdellaoui et al., 2017; Pavlovic et al., 2013), fire retardants (Matusinovic and Wilkie, 2012) drug and herbicide storage and release matrixes (Chaara et al., 2011; Mishra et al., 2018; Rives et al., 2014), electrochemistry (González et al., 2016) biotechnology, (Wang et al., 2014) among many others.

Although LDHs have been widely studied and used as heterogeneous catalysts, but only in recent years, LDHs containing transition metals attracted research interest as photocatalysts (Mohapatra and Parida, 2016; Shao et al., 2011). Many of LDH properties such as uniform distribution of metal cations in the layers, oxo-bridged linkage, high chemical and thermic stability make these materials promissing photocatalysts.

In the field of NOx removal, the use of LDHs has been limited to their use as catalysts for the NO selective reduction or the physical adsorption of NO/NO_2 gas molecules, their use as photocatalysts being almost un-explored. In this sense, we have recently reported on the excellent De-NOx photocatalytic performance and selectivity of ZnAl-CO_3 UV-light-response (Rodriguez-Rivas et al., 2018). However, when considering applications for the environmental remediation of urban atmosphere, the visible light activation of a DeNOx photocatalyst is of importance because the availability of UV light is sometimes limited by urban architecture and geographical/weather conditions (Balbuena et al., 2015). The aim of the present work has been to extend its visible light response by introducing Cr as a LDH dopant, since it has been reported that Cr containing LDHs could be efficient photocatalysts, as the case of decomposition of organic water pollutants (Zhao et al., 2016). Also, Silva et al. (2009) studied a visible active Zn—Cr LDH photocatalysts for oxygen generation from water and observed that a Cr-doped LDH was more active than others. On the other hand, Parida and Mohapatra (Nejati et al., 2018; Parida et al., 2012) reported that the presence of carbonate as the interlayer LDH anion also has a key role in the photocatalytic activity of Zn/Cr–CO_3 for H_2 evolution. These authors state that carbonate is oxidised by positive holes to form carbonate radicals, which reduces the electron/hole recombination.

Concerning the field of DeNOx photochemical processing, here we study the influence of presence and gradual increase of Cr amount in ZnAl-CO_3 LDH as photocatalyst for air remediation. The changes observed in their structural, morphological and optical properties are observed and commented with relation to the enhanced photocatalytic abatement of NOx gases. Moreover, the photochemical oxidation mechanism is explained in the light to the results obtained by using EPR and PL techniques.

2. Materials and methods

The chemicals used in this work were of analytical grade and demineralized water was used in the Experimental section. The $Zn(NO_3)_2{\cdot}6H_2O$, $Al(NO_3){\cdot}9H_2O$ and $Fe(NO_3){\cdot}9H_2O$ salts (purchased from Panreac AppliChem) and 5,5-dimethyl-L-pyrroline-*N*-oxide (DMPO) solution (acquired from Sigma Aldrich) were used without further treatment.

2.1. Synthesis of LDHs

ZnAlCr and ZnCr LDHs samples were prepared, by using the co-precipitation, with different Cr/Al and Cr/Zn ratios. 100 mL of 0.2 M solution of $Zn(NO_3)_2{\cdot}6H_2O$, $Al(NO_3)_3{\cdot}9H_2O$ and $Cr(NO_3)_3{\cdot}9H_2O$ (Zn/Cr and Zn/(Cr + Al) = 3; where Cr/Al = 0, 0.25, 1) was added drop-wise into 100 mL of 0.1 M Na_2CO_3 solution under stirring at room temperature. The constant pH = 10 was kept by dropping a 2.0 M NaOH solution during the coprecipitation reaction. The slurry obtained was then stirred during 1 h, cured during 24 h, centrifuged, washed with distilled water, and dried in an oven at 60 °C. The LDHs prepared were labeled as ZACx.xx, the letter (when it appeared) denoting the initial of the metallic element name, the number denoting the used Cr/Zn ratio.

2.2. Characterization of the photocatalysts

The phase structure of the powder samples was recorded by X-ray diffraction (XRD; Bruker D8 Discovery; λ = 1.5405 Å; step size = 0.02° (2θ); step counting = 0.65 s). Infrared spectra (IR) analysis from 450 to 4000 cm^{-1} was carried out on transmission mode in a FT-MIR Bruker Tensor 27 with a resolution of 1 cm^{-1}. The morphology of the photocatalysts was researched by scanning electron microscopy (SEM) in a Jeol JSM 7800F instrument. The elemental chemical analyses were performed by induced coupled plasma mass spectroscopy (ICP-MS; Perkin Elmer Nexion X). The thermogravimetric analysis (TGA) was performed on a Mettler Toledo equipment in oxygen atmosphere (flow: 100 mL min^{-1}; heating rate: 10 °C min^{-1}).

The pore microstructure and textural properties were studied by N_2 adsorption–desorption isotherms recorded at 77.4 k on a Micromeritics ASAP 2020 apparatus. The Specific surface area of each sample was calculated by applying the Brunauer-Emmet-Teller (BET) measurement in the N_2 adsorption isotherms. Before the measurements, the samples were degassed under vacuum (100 °C for 1 h).

Diffuse reflectance (DR) UV–Vis spectra (rate of 30 nm min^{-1}; step of 0.5 nm) were collected at room temperature with a Varian Cary 1E instrument. The steady-state photoluminescence (PL) emission spectra were collected on a FLS920 Fluorimeter (Edinburgh Instrument Ltd., Livingston, UK). Electron paramagnetic resonance (EPR) spectra, recorded at room temperature in an EMXmicro (Bruker) spectrometer, were conducted three times to quantitatively detect the concentration of $^{\bullet}OH$ or $^{\bullet}O_2^-$ by using 5,5-dimethyl-1-pyrroline-*N*-oxide (DMPO) as spin-trap agent. Thus, the LDH sample was dispersed in a solution (water or methanol for detecting $^{\bullet}OH$ or $^{\bullet}O_2^-$, respectively) with 45 mM DMPO and irradiated during 30 min with a Xe lamp (artificial sunlight).

2.3. Photocatalytic activity evaluation

The photochemical performance of LDHs to abate the NO gas concentration in air was assessed in a laminar flow reactor. The reactor was illuminated using a solar light irradiation box (Solarbox 3000e RH; Xe lamp). The reactor containing the LDHs photocatalyst, 500 mg of sample powder supported in a 5 × 5 cm sample holder, was irradiated with artificial sunlight (irradiances of 25 and 580 Wm^{-2} for UV and visible light). 150 ppb NO polluted air atmosphere was simulated when synthetic air and pure NO were mixed together and sent to the reactor (flow rate gas = 0.30 L min^{-1}). This concentration was selected in order to simulate the high levels of NO concentration, reached in highly populated cities (Kim et al., 2008). A relative humidity of 50 ± 5% was maintained during the experiment. The analysis of nitrogen oxides gases concentration was continuously recorded by a chemiluminescence analyzer (Environment AC3 2 M instrument). For each test, the air/NO gas mixture was passed over the sample in the dark for 30 min (before and after the light irradiation period) to discard the existence of NO_X adsorption. NO photolysis was no observed in light irradiation tests carried out in the absence of the sample. Each DeNOx photocatalytic test was done three times in order to calculate the average concentration values. The photocatalytic NO and NOx removal efficiency and the corresponding selectivity were calculated following the equations:

$$NO\ conversion\ (\%) = \frac{\left([NO]_{in} - [NO]_{out}\right)}{[NO]_{in}} \times 100 \quad (1)$$

$$NOx\ conversion\ (\%) = \frac{([NOx]_{in} - [NOx]_{out})}{[NOx]_{in}} \times 100 \quad (2)$$

$$\text{Selectivity; } S\ (\%) = \frac{([NOx]_{in} - [NOx]_{out})\ /[NOx]_{in}}{([NO]_{in} - [NO]_{out})\ /[NO]_{in}} \times 100 \quad (3)$$

where $[--]_{in}$ represent the measured inlet concentration, $[--]_{out}$ the measured outlet concentration, and $[NO_X]$ the sum of [NO] and $[NO_2]$ concentrations.

3. Results and discussion

3.1. Photocatalyst characterization

Fig. 1 shows the XRD patterns corresponding to the ZnAl-LDH, ZnAlCr-LDH and ZnCr-LDH samples. The non-substituted ZnAl-LDH exhibits diffraction peaks at 11.8°, 23.5°, 34.6°, 39.1°, 46.6°, 60.0°, and 61.4° are assigned to (003), (006), (012), (015), (018), (110) and (113) crystal planes of a layered double hydroxide framework, respectively (Rodriguez-Rivas et al., 2018). The spacing estimated for the d_{003} basal plane, around = 7,61 Å, is indicative of the presence of a carbonate anion in the interlayer of LDH (Crespo et al., 1997). No changes at the 2θ position of the main diffraction peaks are observed with the gradual substitution of Al^{3+} by Cr^{3+}, confirming that LDH structure was preserved. However, the increased presence of Cr^{3+} in the LDH framework provokes a dramatic decrease in the crystallinity of the samples, as inferred from Fig. 1, with smaller and broader diffraction peaks being observed.

The Fourier Transform Infrared (FT-IR) spectra of the four LDHs are shown in Fig. 2. The data obtained confirm the characteristic signal

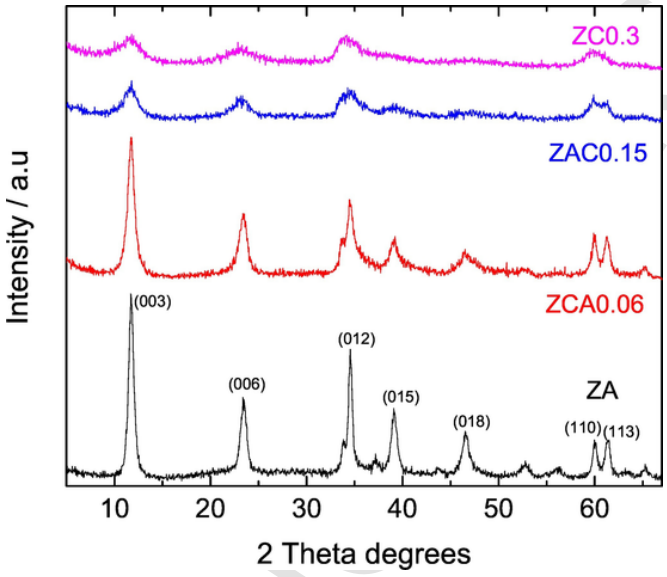

Fig. 1. XRD patterns for the ZnAl-LDH, ZnAlCr-LDH and ZnCr-LDH samples.

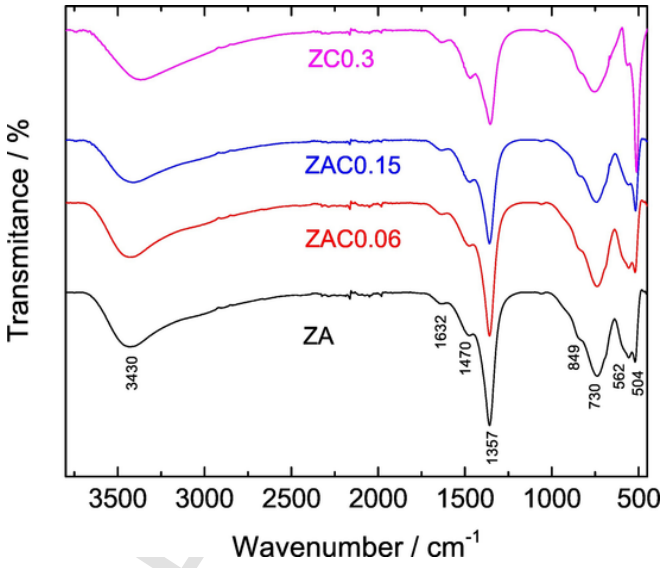

Fig. 2. IR spectra obtained for the ZnAl-LDH, ZnAlCr-LDH and ZnCr-LDH samples.

of a pure LDH phase in all samples (Baliarsingh et al., 2014). The band centered at 3430 cm^{-1}, a broad and strong absorption, indicates the presence of O–H bonds. The weaker band observed at 1639 cm^{-1} is representative of the bending mode of water molecules in the interlayer space. The split asymmetric stretching modes of an interlayer carbonate ion appear at 1357 (the strongest band) and 1475 cm^{-1}. Finally, at lower frequencies, the bands observed at around 741 and 520 cm^{-1} are attributed to the lattice vibration mode in the brucite-like layers of the M–OH and the M–O bonds, respectively. The band at 520 cm^{-1} could be assigned to Cr—O stretching vibration, its intensity increasing with the amount of chromium content (Gutmann and Müller, 1996). Moreover, this band moves with the change in LDH chemical composition, i.e. it shifts towards lower frequencies which could be associated with a distortion of the hydroxide sheets occurs when Al^{3+} is substituted by Cr^{3+} (García-García et al., 2007).

The chemical formula for each LDH compound was proposed based on the data obtained from the chemical analysis and TG analysis, Table 1. For all the samples, the Zn/M^{3+} atomic ratio is practically maintained (around 3.25) independently of the type and amount of each trivalent ion. The positive valence of metallic ions is compensated by hydroxyl and carbonate anions, the latter in the necessary amount to counteract the excess of positive charge caused by the presence of M^{3+} ions in the layers. On the other hand the first weight loss in the thermogravimetric curve was associated with the amount of water molecules, Fig. S1 (Supplementary information).

The morphology of the obtained samples was examined by SEM microscopy, Fig. 3. The ZnAl-LDH sample, ZA, is constituted by well-defined hexagonal sheet-like crystals. This morphology reflects the layered structure observed in the XRD patterns. However, the crystallization becomes poorer with the presence and increase of Cr^{3+} ion in the chemical formulae. Thus, it is observed how the presence of the

Table 1
Chemical and physical characteristics for the prepared LDH samples.

Sample	% Wt			Atomic ratio			Proposed formula	S_{BET}
	Zn	Al	Cr	Zn/M^{3+}	Cr/Al	Cr/Zn		($m^2\ g^{-1}$)
ZA	44.90	5.8	–	3.19	–	–	$[Zn_{0.76}Al_{0.24}(OH)_2](CO_3)_{0.12}{\cdot}0.75\ H_2O$	76
ZAC0.06	44.21	4.64	2.24	3.14	0.25	0.06	$[Zn_{0.76}Al_{0.19}Cr_{0.05}(OH)_2](CO_3)_{0.12}{\cdot}0.75\ H_2O$	87
ZAC0.15	42.57	2.73	5.33	3.34	1.00	0.15	$[Zn_{0.77}Al_{0.115}Cr_{0.115}(OH)_2](CO_3)_{0.115}{\cdot}0.79\ H_2O$	108
ZC0.3	41.42	–	9.97	3.30	–	0.30	$[Zn_{0.77}Cr_{0.23}(OH)_2](CO_3)_{0.115}{\cdot}0.98\ H_2O$	112

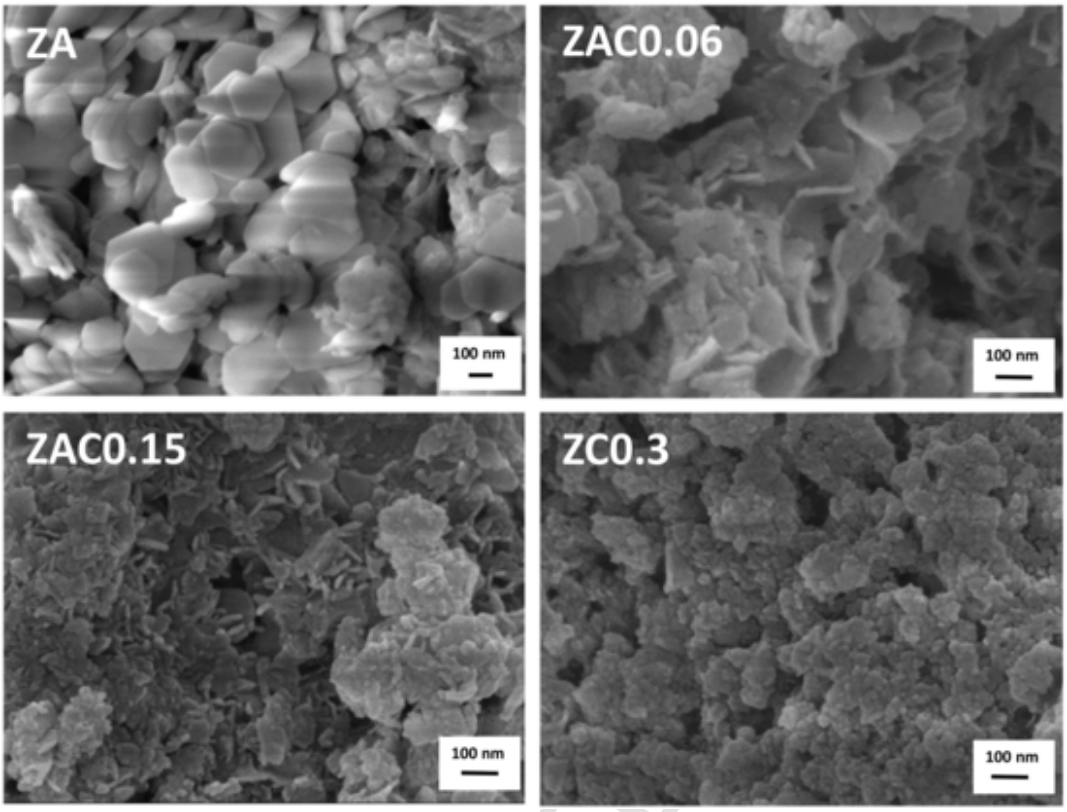

Fig. 3. SEM images for the ZnAl-LDH, ZnAlCr-LDH and ZnCr-LDH samples.

pseudo hexagonal sheets becomes minor in the sample ZAC0.06, scarce in the sample ZAC0.15 and is absent in the sample ZC0.3 which is constituted by aggregates of nanometric unshaped nanoparticles. The lower crystallinity observed in Cr^{3+} containing samples, which is also reflected in the corresponding XRD patterns (Fig. 1), could be due to the more acidic character of Cr salt containing solutions, compared to those of Al containing ones, which could decrease the homogeneity of the suspension being determinant in the textural characteristics of the samples.

In order to know about the potential reactivity as photocatalysts of the LDHs here studied, additional characterization concerning the surface area and the light activation was performed. The N_2 adsorption-desorption isotherm of the samples, Fig. 4, was used to determine the specific surface area and porous structure. Following the IUPAC classification (Sing et al., 1985) and in similarity with previous studies on LDHs (Carriazo et al., 2011; Extremera et al., 2012; Rodriguez-Rivas et al., 2018) a type II isotherm shape was obtained for ZA sample with a contribution of type IV. This shape is characteristic of the adsorption on macro-porous and non-porous materials. The type H3 hysteresis loop corresponds to the presence of mesopores, as inferred from the pore size distribution (Fig. S2). In agreement with the observed change originated in the morphology, the increase in chromium content alters the porous structure. The H3 loop, appearing in plate-like particles aggregates giving rise to slit-like pores, gradually changes to H4 type, which corresponds to narrow slit-like pores (Sing et al., 1985). Moreover, an increase in the amount of mesopores <20 nm in size is observed. Therefore, the change in porosity is in accordance with the change accounted in the morphology of the LDHs crystals. Table 1 shows the specific surface areas measured by BET method. The BET values increased for Cr substituted samples in agreement with their lower crystallinity as was confirmed by XRD (Fig. 1) and SEM characterization (Fig. 3). The ZC0.3 sample exhibited an expanded specific surface area of 112 $m^2\,g^{-1}$, around 50% superior to that of the non-substituted ZA sample, and highly superior to those previously reported for ZnCr-LDH (Baliarsingh et al., 2013; Koilraj and Kannan, 2013; Paušová et al., 2015).

The light absorption properties of the ZnAl, ZnAlCr and ZnCr LDHs were studied by DR UV–Vis spectroscopy, Fig. 5. The absorption spectrum obtained for the ZA sample is that expected for Zn—Al LHDs (Ahmed et al., 2012), with a main intense absorption peak at $\lambda < 250$ nm and a smaller one at 300 nm, both in the UV light range. The incorporation of Cr^{3+} ions to the LDH framework results in the apparition of two strong absorption peaks located at 409 and 567 nm, with intensity increasing with the Cr^{3+} content. These peaks correspond to d-d transition of trivalent chromium ions octahedrally coordinated in the LDH structure (Gunjakar et al., 2011; Zhao et al., 2011). The broad and intense absorption bands in the 350–800 nm range suggest their potential utilization as visible light active photocatalysts.

3.2. Photocatalytic De-NOx behaviour and mechanism

The photocatalytic ability of the ZnAl, ZnAlCr and ZnCr LDHs to remove NO gas was studied as follows. Fig. 6a shows a representative plot of the nitrogen oxides concentration changes measured during the photocatalytic test. Before light irradiation no physico-chemical interaction of NO gas with the photocatalyst was observed, as inferred from the constant value of gas concentration measured during the first 30 min. Once the sunlight lamp was turned on, the NO concentration decreased suddenly and the NO removal rapidly increased on time. As previously reported (Rodriguez-Rivas et al., 2018), and discussed here below, once the LDH particles are light activated, e^- and h^+ charges are produced which initiate the reactions leading to the progressive oxidation of NO gas. After the first 20 min of light irradiation the photo-oxidation activity became stable, as the NO concentration reached a constant value. The nitrogen oxide levels quickly returned to the original inlet concentration when illumination was shut down.

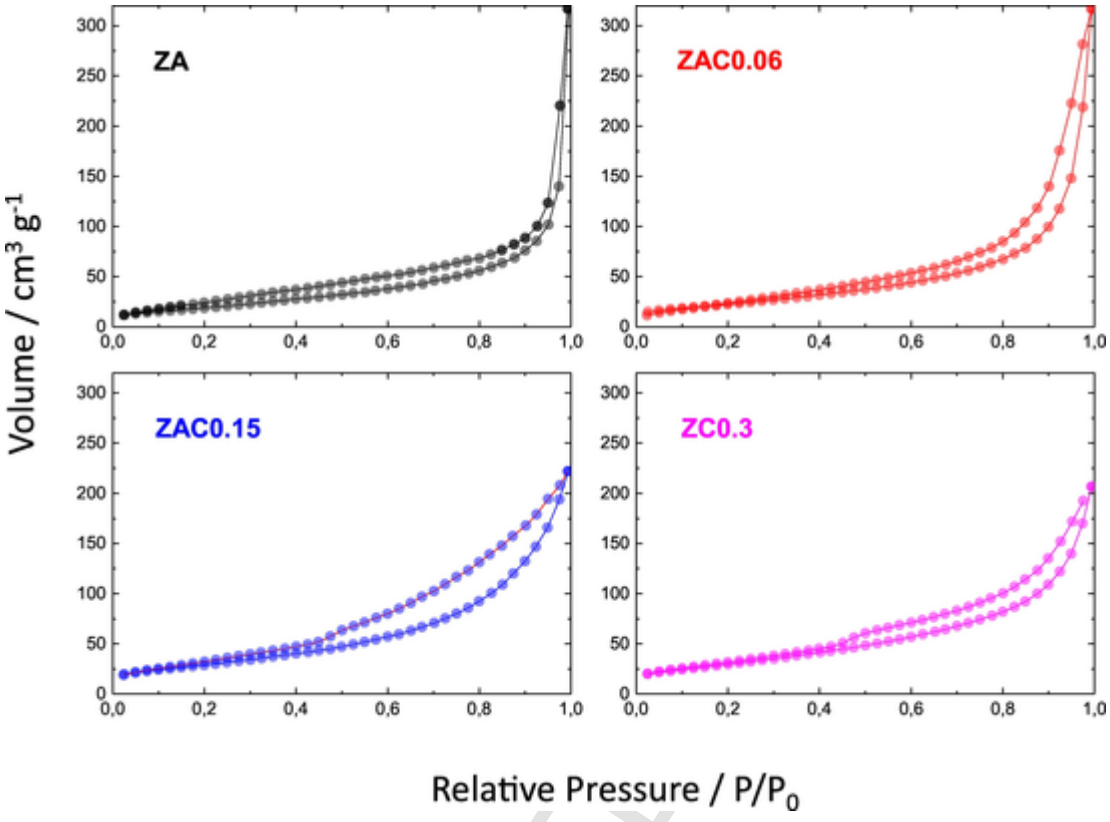

Fig. 4. N_2 adsorption-desorption isotherms for the ZnAl-LDH, ZnAlCr-LDH and ZnCr-LDH samples.

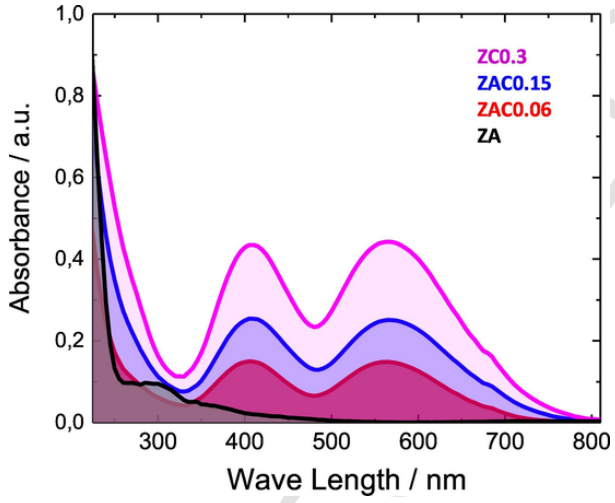

Fig. 5. The UV–Vis absorption spectra for the ZnAl-LDH, ZnAlCr-LDH and ZnCr-LDH samples.

Fig. 6b shows the differences found for the NO abatement when ZnAl, ZnAlCr and ZnCr photocatalysts are used. As the content of chromium increased in the LDH sample, better NO removal efficiencies were obtained. Thus, a value of 55% was measured for the ZC0.3 sample in comparison to that of 44% for the ZA sample. In Fig. 6c, it can be observed that a similar amount of nitrogen dioxide molecules were released during the experiment, around 7–9 ppb, regardless of the photocatalyst used. The NO_2 gas appears as an intermediate during the NO photochemical oxidation (Balbuena et al., 2015) which must be avoided because it is much more dangerous than NO (Lewis and Sax, 2012). Taking into account the above values, the selectivity of the De-NOx process (*S*) is estimated at around 90% for all the photocatalysts here studied, an outstanding value in line with those reported for the last advanced De-NOx photocatalysts recently reported (Balci Leinen et al., 2019; Folli et al., 2011; Pastor et al., 2019; Shang et al., 2019; Tan et al., 2017).

The enhanced photochemical De-NOx behaviour must be related with the changes induced by the presence of Cr^{3+} ions in the LDH framework. Thus, the increased surface area exhibited in samples containing Cr^{3+} allowed an easier accessibility of gas molecules to the photo-active centres, which should result in a more efficient photochemical process. On the other hand, thanks to the presence of Cr^{3+} ions, the Vis light activation was highly relevant to the measured photochemical De-NOx activity. In Fig. 6d, the NO abatement measured for the samples only under visible light ($\lambda > 410$ nm) is shown. The response obtained for the ZA sample is almost negligible and responds to the small tail between 400 and 450 nm observed in the corresponding UV–Vis absorbance spectra (Fig. 5). However, the removal of NO increased with the content of chromium. This is indicative that, under visible light, the chromium centres are those responsible for the light absorption and the photochemical oxidation process. The low NO abatement index found, between 10 and 15% after 60 min of light irradiation, is in concordance with the lower presence of Cr (3 to 13 times) than that of Zn in the LDH formulae.

For practical considerations the sample ZC0.3, which exhibited the best photochemical NO abatement, was studied in long term irradiation and reusability experiments. Fig. 6e shows the nitrogen oxide concentration changes measured during the photocatalytic test when the irradiation time is extended for 6 h. This period of time is similar to that in which the daytime mean values of NO concentration in a highly populated city reach their maximum level (Kim et al., 2008). It can be observed that NO abatement is higher in the first 60 min and slowly decreases with time to reach a 47% removal efficiency at the end of the experiment. Interestingly, only 8 ppb of NO_2 concentration was measured during the whole test, confirming the outstanding high selectiv-

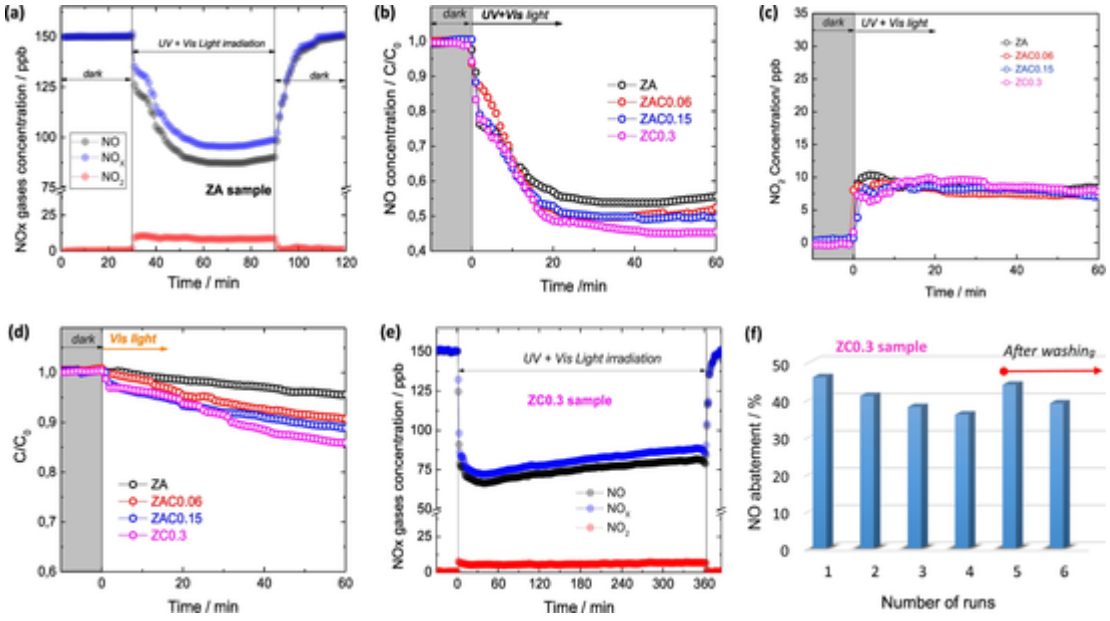

Fig. 6. (a) NOx gas concentration evolution during the photo-degradation of gaseous NO under UV–Vis light irradiation on the ZnAl-LDH sample. (b) Photo-oxidative removal of NO and (c) NO_2 gas concentration measured under UV–Vis light irradiation on ZnAl-LDH, ZnAlCr-LDH and ZnCr-LDH catalysts. (d) Photo-oxidative removal of NO under Visible light irradiation. (e) NOx gas concentration evolution during the photo-degradation of gaseous NO under 6 h of UV–Vis light irradiation on the ZC0.3 sample. (f) NO removal efficiency calculated for each run of the reusability tests for the ZC0.3 sample.

ity inherent on these LDH photocatalysts (Rodriguez-Rivas et al., 2018). The declined NO removal efficiency on time is related to the fact that nitrate species, the final product of NO oxidation, are being deposited on the surface of the catalyst hidden the photo-active centres to the reactant gas molecules. In fact, this decrease in efficiency becomes higher when the photocatalytic test is performed several successive times on the same sample. Thus, the Fig. 6f shows the percentage of NO removal obtained in consecutive trial performed with the sample ZC0.3, the photocatalyst being irradiated for 6 h in each essay. Due to the nitrate accumulation on the photocatalyst surface, the efficiency decreases in each run. The sample was washed with milli-Q water after the fourth run, to eliminate the existence of nitrates from the particles surface. In the following experiments, runs number 5 and 6, the initial photocatalytic performance is recovered. These tests guarantee the reusability of the ZnCr0.3 photocatalyst after long term experiences, exhibiting an average NO abatement index of around 40%.

The above commented results are better understood once the corresponding photochemical mechanism is taken into consideration. The proposed mechanism for the photochemical oxidation of NO molecules, involving several steps and different intermediate species (Balbuena et al., 2015; Devahasdin et al., 2003), is similar to that found for several De-NOx photocatalysts such as TiO_2, Fe_2O_3, ZnO, CN among others (Balbuena et al., 2015; Sugrañez et al., 2015; Wang et al., 2019; Wei et al., 2013), summarized here as follows:

$$Zn/Cr-LDH + h\nu \rightarrow Zn/Cr-LDH^{*}\ \left(h_{vb}^{+} + e_{cb}^{-}\right) \quad (4)$$

$$h_{vb}^{+} + H_2O \rightarrow {}^{\cdot}OH + H^{+} \quad (5)$$

$$e_{cb}^{-} + O_2 \rightarrow {}^{\cdot}O_2^{-} \quad (6)$$

$${}^{\cdot}O_2^{-} + H^{+} \rightarrow {}^{\cdot}OOH \quad (7)$$

$$NO + 2{}^{\cdot}OH \rightarrow NO_2 + H_2O \quad (8)$$

$$NO_2 + {}^{\cdot}OH \rightarrow NO_3^{-} + H^{+} \quad (9)$$

$$NO_X + {}^{\cdot}O_2^{-} \rightarrow NO_3^{-} \quad (10)$$

The PCO process initiates when the LDH particles absorb light. Once the photocatalyst receives the photon energy (Eq. (4)), the electron transfer from the valence to the conduction band is initiated (Chen et al., 2019). Thus, e^- and h^+ reach the surface of the semiconductor particles (Xia et al., 2013; Xu et al., 2015) producing reactive oxygen species (ROS) from the adsorbed water and oxygen molecules (Eqs. (5)–(7)), which initiate the progressive oxidation of nitrogen oxide gases (Eqs. (8)–(10)).

In regard to the products obtained during the PCO process performed with the ZnCr-LDH photocatalyst, the presence of NO_2 was clearly detected by the chemiluminescence analyzer, as shown in Fig. 6a, c and e. In order to identify the presence of nitrate species the FT-IR technique was used. Fig. S3 shows the three IR spectra obtained: the first one corresponding to the ZC0.3 sample, the second one after the photocatalytic De-NOx test (performed for 6 h of light irradiation) and finally that obtained once the sample collected after the photocatalytic test had been subjected to a washing procedure. The first observation concerns the main bands registered which were similar in the three patterns, indicating that the chemical structure was preserved after photocatalysis or the washing procedure. A detailed observation of the main band at frequencies higher than 1300 cm^{-1}, Fig. 7, shows the appearance of a narrow peak at 1383 cm^{-1} in the pattern recorded on the sample after the photocatalytic test. This band, absent in the pristine sample, corresponds to the N—O stretching vibrations of NO_3^- (Ai et al., 2010; Pastor et al., 2019), confirming that the full photocatalytic oxidation of NO had taken. Therefore, it seems reasonable that the accumulation of nitrate on the photocatalyst surface was the reason for the decay in the NO removal efficiency on time and in repetitive runs. In fact, the absence of this band in the pattern for the sample washed after the De-NOx experiment (Fig. 7), indicates that the nitrate specie was easily eliminated, and without its presence the photocatalytic efficiency is recovered, as indicated in Fig. 6f.

Additionally, the generation of $^{\bullet}OH$ and $^{\bullet}O_2^-$ radicals from the LDH photocatalysts was assessed by EPR measurements using DMPO as the spin-trapping agent under sunlight excitation (Huang et al., 2017). In aqueous solution, the characteristic signal of DMPO-$^{\bullet}OH$ adduct constituted by quartet peaks featuring a 1:2:2:1 intensity ratio was ob-

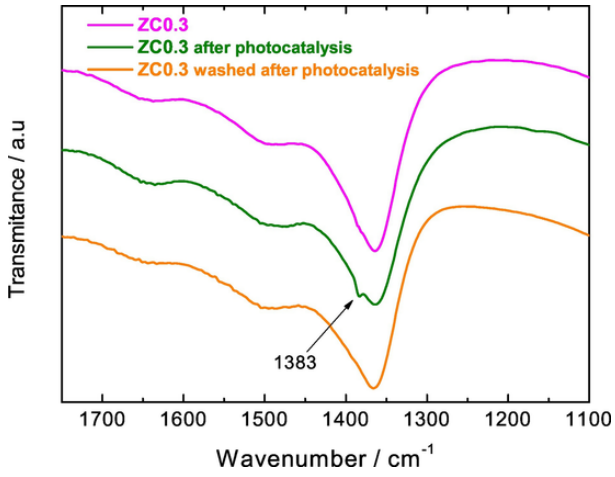

Fig. 7. IR spectra obtained for the ZC0.3 sample before and after De-NOx test.

served, Fig. 8a. Moreover, in the methanol solution, six peaks for the DMPO-$^{\bullet}O_2^-$ adduct were observed, Fig. 8b (Zhao et al., 2011). No signal was detected when the photocatalyst suspension was in the dark. Therefore, the active radicals are formed once the samples are light irradiated. The intensity of the signals registered was higher for the samples containing chromium, slightly increasing in the samples with its presence. Thus, the Cr^{3+} doping enhances the ability to generate active radicals on these samples.

On the other hand, apart from the physical changes mentioned before, we go into further depth to investigate the role of Cr^{3+} ions in the electronic properties of LDH. The photoluminescence spectroscopy is useful in the study of the photocharge generation, transfer and separation efficiency of LDH photocatalysts (Gunjakar et al., 2013; Zhao et al., 2016, 2014). To this respect, the photoluminescence (PL) spectra were recorded for the ZnAl, ZnAlCr and ZnCr LDHs samples, Fig. 9a. A broad PL peak was detected in all samples centered around 425 nm, in concordance with that previously reported in Zn—Cr LDHs (Baliarsingh et al., 2014). For practical applications, large surface charge transfer and low e^-/h^+ recombination properties are required for a photocatalyst. The ZnAl-LDH exhibited the highest PL intensity among the different samples under an excitation wavelength of 360 nm. The high measured intensity is indicative of the large radiative recombination rate of the electrons and holes in the semiconductor, a competitive pathway with the reaction of the photogenerated charges with O_2 and H_2O molecules to form the ROS (Hu et al., 2018). For the samples here studied, the increased Cr^{3+} ion content in the LDH formulae causes a decrease in the PL signal. This behaviour clearly indicates that chromium centres are participating in a new deactivation pathway of the photocharges lessening the recombination of charge carriers. In fact, it is reported that CrO_6 octahedron dispersion in the LDH matrix promotes the efficiency of the excited electron and minimizes the e^-/h^+ recombination, playing a significant role in the photocat-

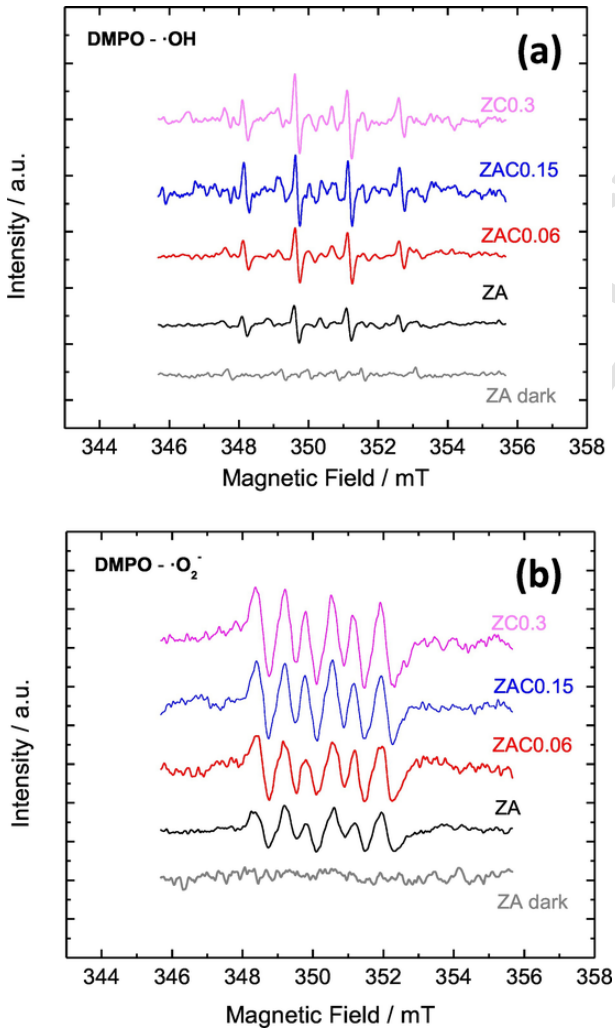

Fig. 8. DMPO spin-trapping EPR spectra of the ZnAl-LDH, ZnAlCr-LDH and ZnCr-LDH samples under UV–Vis light irradiation in (a) aqueous solution for $^{\bullet}OH$ and (b) methanol solution for $^{\bullet}O_2^-$.

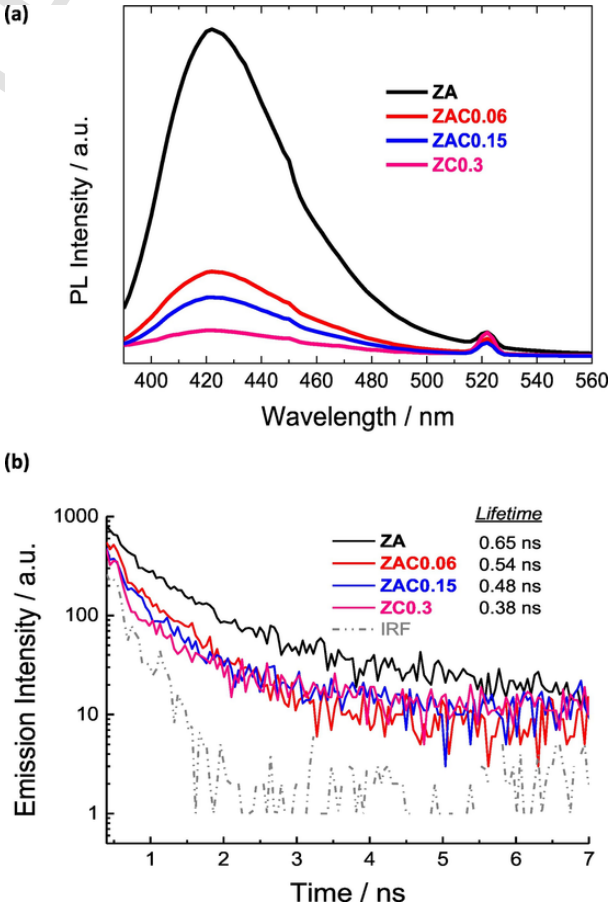

Fig. 9. (a) Photoluminescence (PL) spectra (excitation wavelength = 360 nm) of the different samples. (b) Time decay of the PL signals for the four samples showing the lifetimes obtained with a monoexponential fit. The Instrumental Response Function (IRF) of the instrument is also shown (dotted-dashed grey line).

alytic processes (Baliarsingh et al., 2013; Gunjakar et al., 2013; Zhao et al., 2011). Fig. 9b displays the time decay of the PL signal for the different samples. The decays are much shorter in the case of the samples containing the Cr^{3+} ion, which agrees with the decreased signal of the steady-state experiments. A monoexponential fit of the decays provided PL lifetimes of 0.65 ns for the ZnAl-LDH samples and 0.54, 0.48 and 0.38 ns for three samples with increasing Cr^{3+} content. All these results corroborate the appearance of a new deactivation pathway associated with the transfer of photogenerated charges to the chromium centres. The fact that the electron-hole pair recombination is lessened in chromium containing samples explains its higher ability found in the generation of active radicals (Fig. 8).

4. Conclusions

Different LDHs were prepared by co-precipitation method, with a molar ratio of $Zn^{2+}/M^{3+} = 3$ ($M^{3+} = Al^{3+} + Cr^{3+}$), without Cr and increasing the presence of Cr^{3+} in the LDH framework in the 0.06, 0.15 and 0.3 Cr/Zn ratio. The XRD and FTIR patterns of all the prepared samples showed the presence of pure LDH phase with carbonate anions in the interlamellar space.

The morphological and textural characteristics of LDH containing chromium were markedly different. The crystallinity becomes poorer and the specific surface area higher when the presence of Cr^{3+} increases, presenting values of 112 $m^2\ g^{-1}$ for the ZnCr-LDH and 76 $m^2\ g^{-1}$ for the ZnAl-LDH samples measured. Moreover, the chromium centres are responsible for the absorption of visible light from 350 to 750 nm.

The photochemical mechanism is composed of the NO → NO_2 → NO_3^- sequential steps, a process that only took place in chromium samples under visible light. The PL spectra of the samples show that the presence of the chromium centres in the LDH framework decreases the recombination rate of the electrons and holes, being their ability to form $^{\bullet}OH$ and $^{\bullet}O_2^-$ radicals higher to that of ZnAl-LDH.

The surface area, the expanded range of light activation and the lessened e^-/h^+ recombination characteristics of Cr-containing LDH samples are responsible of the improvement in the photo-oxidative elimination of NO when used as photocatalysts. The sample with the highest amount of Cr^{3+} exhibited a high NO removal efficiency (55%), outstanding selectivity (90%) and good reusability, favouring its potential use as a photocatalyst in the remediation of polluted urban air atmosphere.

Declaration of competing interest

The authors declare that they have no known competing financial interests or personal relationships that could have appeared to influence the work reported in this paper.

Acknowledgements

The authors acknowledge the funding received from the Junta de Andalucía, The Spanish Government (MAT2017-88284-P and CTQ2017-84221-R), the Fundación Carolina and the Ministerio de Educación, Cultura y Deporte (FPU16/05041) which supported this work.

Appendix A. Supplementary data

Supplementary data to this article can be found online at https://doi.org/10.1016/j.scitotenv.2019.136009.

References

Abdellaoui, K., Pavlovic, I., Bouhent, M., Benhamou, A., Barriga, C., 2017. A comparative study of the amaranth azo dye adsorption/desorption from aqueous solutions by layered double hydroxides. Appl. Clay Sci. 143, 142–150. doi:10.1016/J.CLAY.2017.03.019.

Ahmed, A.A.A., Talib, Z.A., Bin Hussein, M.Z., Zakaria, A., 2012. Zn-Al layered double hydroxide prepared at different molar ratios: preparation, characterization, optical and dielectric properties. J. Solid State Chem. 191, 271–278. doi:10.1016/j.jssc.2012.03.013.

Ai, Z., Zhang, L., Lee, S., 2010. Efficient visible light photocatalytic oxidation of NO on aerosol flow-synthesized nanocrystalline $InVO_4$ hollow microspheres. J. Phys. Chem. C 114, 18594–18600. doi:10.1021/jp106906s.

Balbuena, J., Cruz-Yusta, M., Sánchez, L., 2015. Nanomaterials to combat NOx pollution. J. Nanosci. Nanotechnol. 15, 6373–6385. doi:10.1166/jnn.2015.10871.

Balbuena, J., Calatayud, J.M., Cruz-Yusta, M., Pardo, P., Martín, F., Alarcón, J., Sánchez, L., 2018. Mesocrystalline anatase nanoparticles synthesized using a simple hydrothermal approach with enhanced light harvesting for gas-phase reaction. Dalt. Trans. 47, 6590–6597. doi:10.1039/C8DT00721G.

Balbuena, J., Cruz-Yusta, M., Pastor, A., Sánchez, L., 2018. α-Fe_2O_3/SiO_2composites for the enhanced photocatalytic NO oxidation. J. Alloys Compd. 735. doi:10.1016/j.jallcom.2017.11.259.

Balci Leinen, M., Dede, D., Khan, M.U., Çağlayan, M., Koçak, Y., Demir, H.V., Ozensoy, E., 2019. CdTe quantum dot-functionalized P25 titania composite with enhanced photocatalytic NO_2 storage selectivity under UV and Vis irradiation. ACS Appl. Mater. Interfaces 11, 865–879. doi:10.1021/acsami.8b18036.

Baliarsingh, N., Mohapatra, L., Parida, K., 2013. Design and development of a visible light harvesting Ni-Zn/Cr-CO_3^{2-} LDH system for hydrogen evolution. J. Mater. Chem. A 1, 4236–4243. doi:10.1039/c2ta00933a.

Baliarsingh, N., Parida, K.M., Pradhan, G.C., 2014. Effects of Co, Ni, Cu, and Zn on photophysical and photocatalytic properties of carbonate intercalated M^{II}/Cr LDHs for enhanced photodegradation of methyl orange. Ind. Eng. Chem. Res. 53, 3834–3841. doi:10.1021/ie403769b.

Boningari, T., Smirniotis, P.G., 2016. Impact of nitrogen oxides on the environment and human health: Mn-based materials for the NOx abatement. Curr. Opin. Chem. Eng. 13, 133–141. doi:10.1016/j.coche.2016.09.004.

Carriazo, D., Del Arco, M., García-López, E., Marc, G., Martín, C., Palmisano, L., Rives, V., 2011. Zn,Al hydrotalcites calcined at different temperatures: preparation, characterization and photocatalytic activity in gas-solid regime. J. Mol. Catal. A Chem. 342–343, 83–90. doi:10.1016/j.molcata.2011.04.015.

Cavani, F., Trifiro, F., Vaccari, A., 1991. Hydrotalcite-type anionic clays: preparation, properties and applications. Catal. Today 11, 173–301. doi:10.1016/0920-5861(91)80068-K.

Chaara, D., Bruna, F., Ulibarri, M.A., Draoui, K., Barriga, C., Pavlovic, I., 2011. Organo/layered double hydroxide nanohybrids used to remove non ionic pesticides. J. Hazard. Mater. 196, 350–359. doi:10.1016/j.jhazmat.2011.09.034.

Chen, F., Huang, H., Guo, L., Zhang, Y., Ma, T., 2019. The role of polarization in photocatalysis. Angew. Chemie - Int. Ed. 58, 10061–10073. doi:10.1002/anie.201901361.

Crespo, I., Barriga, C., Rives, V., Ulibarri, M.A., 1997. Intercalation of iron hexacyano complexes in Zn,Al-hydrotalcite. Solid State Ionics 101–103, 729–735. doi:10.1016/s0167-2738(97)00290-7.

Devahasdin, S., Fan, C., Li, K., Chen, D.H., 2003. TiO_2 photocatalytic oxidation of nitric oxide: transient behavior and reaction kinetics. J. Photochem. Photobiol. A Chem. 156, 161–170. doi:10.1016/S1010-6030(03)00005-4.

E.C. Agency, 2017. ANNEX 2, Comments and Response to Comments on CLH Proposal on Titanium Dioxide.

Extremera, R., Pavlovic, I., Pérez, M.R., Barriga, C., 2012. Removal of acid orange 10 by calcined Mg/Al layered double hydroxides from water and recovery of the adsorbed dye. Chem. Eng. J. 213, 392–400. doi:10.1016/j.cej.2012.10.042.

Fan, G., Li, F., Evans, D.G., Duan, X., 2014. Catalytic applications of layered double hydroxides: recent advances and perspectives. Chem. Soc. Rev. 43, 7040–7066. doi:10.1039/c4cs00160e.

Folli, A., Campbell, S.B., Anderson, J.A., MacPhee, D.E., 2011. Role of TiO_2 surface hydration on NO oxidation photo-activity. J. Photochem. Photobiol. A Chem. 220, 85–93. doi:10.1016/j.jphotochem.2011.03.017.

Frampton, M.W., Greaves, I.A., 2009. NOx - NOx: who's there? Am. J. Respir. Crit. Care Med. 179, 1077–1078. doi:10.1164/rccm.200903-0485ED.

García-García, J.M., Pérez-Bernal, M.E., Ruano-Casero, R.J., Rives, V., 2007. Chromium and yttrium-doped magnesium aluminum oxides prepared from layered double hydroxides. Solid State Sci. 9, 1115–1125. doi:10.1016/j.solidstatesciences.2007.07.029.

González, M.A., Trócoli, R., Pavlovic, I., Barriga, C., La Mantia, F., 2016. Layered double hydroxides as a suitable substrate to improve the efficiency of Zn anode in neutral pH Zn-ion batteries. Electrochem. Commun. 68, 1–4. doi:10.1016/j.elecom.2016.04.006.

Gunjakar, J.L., Kim, T.W., Kim, H.N., Kim, I.Y., Hwang, S.J., 2011. Mesoporous layer-by-layer ordered nanohybrids of layered double hydroxide and layered metal oxide: highly active visible light photocatalysts with improved chemical stability. J. Am. Chem. Soc. 133, 14998–15007. doi:10.1021/ja203388r.

Gunjakar, J.L., Kim, T.W., Kim, I.Y., Lee, J.M., Hwang, S.J., 2013. Highly efficient visible light-induced O_2 generation by self-assembled nanohybrids of inorganic nanosheets and polyoxometalate nanoclusters. Sci. Rep. 3, 1–8. doi:10.1038/srep02080.

Gutmann, N., Müller, B., 1996. Insertion of the dinuclear dihydroxo-bridged Cr(III) aquo complex into the layered double hydroxides of hydrotalcite-type. J. Solid State Chem. 122, 214–220. doi:10.1006/jssc.1996.0104.

He, S., An, Z., Wei, M., Evans, D.G., Duan, X., 2013. Layered double hydroxide-based catalysts: nanostructure design and catalytic performance. Chem. Commun. 49, 5912–5920. doi:10.1039/c3cc42137f.

Hu, J., Chen, D., Li, N., Xu, Q., Li, H., He, J., Lu, J., 2018. Fabrication of graphitic-C_3N_4 quantum dots/graphene-$InVO_4$ aerogel hybrids with enhanced photocatalytic NO removal under visible-light irradiation. Appl. Catal. B Environ. 236, 45–52. doi:10.1016/j.apcatb.2018.04.080.

Huang, H., Tu, S., Zeng, C., Zhang, T., Reshak, A.H., Zhang, Y., 2017. Macroscopic polarization enhancement promoting photo- and piezoelectric-induced charge separation and molecular oxygen activation. Angew. Chemie - Int. Ed. 56, 11860–11864. doi:10.1002/anie.201706549.

Kim, K.H., Pandey, S.K., Nguyen, H.T., Chung, S.Y., Cho, S.J., Kim, M.Y., Oh, J.M., Sunwoo, Y., 2008. Long-term behavior of particulate matters at urban roadside and background locations in Seoul, Korea. Transp. Res. Part D Transp. Environ. 15, 168–174. doi:10.1016/j.trd.2009.12.001.

Koilraj, P., Kannan, S., 2013. Aqueous fluoride removal using ZnCr layered double hydroxides and their polymeric composites: batch and column studies. Chem. Eng. J. 234, 406–415. doi:10.1016/j.cej.2013.08.101.

Lee, J.H., Wu, C.F., Hoek, G., de Hoogh, K., Beelen, R., Brunekreef, B., Chan, C.C., 2014. Land use regression models for estimating individual NOx and NO_2 exposures in a metropolis with a high density of traffic roads and population. Sci. Total Environ. 472, 1163–1171. doi:10.1016/j.scitotenv.2013.11.064.

Lewis, R.J., Sax, N.I., 2012. Sax's Dangerous Properties of Industrial Materials. twelfth ed. (New York).

Ma, J., Wu, H., Liu, Y., He, H., 2014. Photocatalytic removal of NOx over visible light responsive. J. Phys. Chem. C 118, 7434–7441. doi:10.1021/jp500116n.

Matusinovic, Z., Wilkie, C.A., 2012. Fire retardancy and morphology of layered double hydroxide nanocomposites: a review. J. Mater. Chem. 22, 18701–18704. doi:10.1039/c2jm33179a.

Mishra, G., Dash, B., Pandey, S., 2018. Layered double hydroxides: a brief review from fundamentals to application as evolving biomaterials. Appl. Clay Sci. 153, 172–186. doi:10.1016/j.clay.2017.12.021.

Mohapatra, L., Parida, K., 2016. A review on the recent progress, challenges and perspective of layered double hydroxides as promising photocatalysts. J. Mater. Chem. A 4, 10744–10766. doi:10.1039/C6TA01668E.

Nejati, K., Akbari, A.R., Davari, S., Asadpour-Zeynali, K., Rezvani, Z., 2018. Zn–Fe-layered double hydroxide intercalated with vanadate and molybdate anions for electrocatalytic water oxidation. New J. Chem. doi:10.1039/C7NJ04469K.

Parida, K., Mohapatra, L., Baliarsingh, N., 2012. Effect of Co^{2+} substitution in the framework of carbonate intercalated Cu/Cr LDH on structural, electronic, optical, and photocatalytic properties. J. Phys. Chem. C 116, 22417–22424. doi:10.1021/jp307353f.

Pastor, A., Balbuena, J., Cruz-Yusta, M., Pavlovic, I., Sánchez, L., 2019. ZnO on rice husk: a sustainable photocatalyst for urban air purification. Chem. Eng. J. 368, 659–667. doi:10.1016/j.cej.2019.03.012.

Paušová, Š., Krýsa, J., Jirkovský, J., Forano, C., Mailhot, G., Prevot, V., 2015. Insight into the photocatalytic activity of ZnCr-CO_3 LDH and derived mixed oxides. Appl. Catal. B Environ. 170–171, 25–33. doi:10.1016/j.apcatb.2015.01.029.

Pavlovic, I., González, M.A., Rodríguez-Rivas, F., Ulibarri, M.A., Barriga, C., 2013. Caprylate intercalated layered double hydroxide as adsorbent of the linuron, 2,4-DB and metamitron pesticides from aqueous solution. Appl. Clay Sci. 80–81, 76–84. doi:10.1016/j.clay.2013.06.008.

Peel, J.L., Haeuber, R., Garcia, V., Russell, A.G., Neas, L., 2013. Impact of nitrogen and climate change interactions on ambient air pollution and human health. Biogeochemistry 114, 121–134. doi:10.1007/s10533-012-9782-4.

Rives, V., del Arco, M., Martín, C., 2014. Intercalation of drugs in layered double hydroxides and their controlled release: a review. Appl. Clay Sci. 88–89, 239–269. doi:10.1016/j.clay.2013.12.002.

Rodriguez-Rivas, F., Pastor, A., Barriga, C., Cruz-Yusta, M., Sánchez, L., Pavlovic, I., 2018. Zn-Al layered double hydroxides as efficient photocatalysts for NOx abatement. Chem. Eng. J. 346, 151–158. doi:10.1016/j.cej.2018.04.022.

Sax, N.I., Lewis, R.J., 2012. Sax's Dangerous Properties of Industrial Materials. 12th ed. Van Nostrand Reinhold, New York. ed.

Shang, H., Li, M., Li, H., Huang, S., Mao, C., Ai, Z., Zhang, L., 2019. Oxygen vacancies promoted the selective photocatalytic removal of NO with blue TiO_2 via simultaneous molecular oxygen activation and photogenerated hole annihilation. Environ. Sci. Technol. 53, 6444–6453. doi:10.1021/acs.est.8b07322.

Shao, M., Han, J., Wei, M., Evans, D.G., Duan, X., 2011. The synthesis of hierarchical Zn-Ti layered double hydroxide for efficient visible-light photocatalysis. Chem. Eng. J. 168, 519–524. doi:10.1016/j.cej.2011.01.016.

Silva, C.G., Bouizi, Y., Fornés, V., García, H., 2009. Layered double hydroxides as highly efficient photocatalysts for visible light oxygen generation from water. J. Am. Chem. Soc. 131, 13833–13839. doi:10.1021/ja905467v.

Sing, K.S.W., Everett, D.H., Haul, R.A.W., Moscou, L., Pierotti, R.S., Rouquerol, J., Siemieniewska, T., 1985. International Union of Pure Commission on Colloid and Surface Chemistry including catalysis - reporting physisorption data for gas/solid systems with special reference to the determination of surface area and porosity. Pure Appl. Chem. 57, 603–619. doi:10.1351/pac198557040603.

Sugrañez, R., Balbuena, J., Cruz-yusta, M., Martín, F., Morales, J., Sánchez, L., 2015. Efficient behaviour of hematite towards the photocatalytic degradation of NOx gases. Appl. Catal. B Environ. 165, 529–536. doi:10.1016/j.apcatb.2014.10.025.

Tan, B., Zhang, X., Li, Y., Chen, H., Ye, X., Wang, Y., Ye, J., 2017. Anatase TiO_2 mesocrystals: green synthesis, in situ conversion to porous single crystals, and self-doping Ti^{3+} for enhanced visible light driven photocatalytic removal of NO. Chem. Eur. J. 23, 5478–5487. doi:10.1002/chem.201605294.

Wang, J., Zhu, R., Gao, B., Wu, B., Li, K., Sun, X., Liu, H., Wang, S., 2014. The enhanced immune response of hepatitis B virus DNA vaccine using SiO_2@LDH nanoparticles as an adjuvant. Biomaterials 35, 466–478. doi:10.1016/j.biomaterials.2013.09.060.

Wang, Z., Huang, Y., Chen, M., Shi, X., Zhang, Y., Cao, J., Ho, W., Lee, S.C., 2019. Roles of N-vacancies over porous g-C_3N_4 microtubes during photocatalytic NOx removal. ACS Appl. Mater. Interfaces 11, 10651–10662. doi:10.1021/acsami.8b21987.

Wei, Y., Huang, Y., Wu, J., Wang, M., Guo, C., Qiang, D., Yin, S., Sato, T., 2013. Synthesis of hierarchically structured ZnO spheres by facile methods and their photocatalytic deNOx properties. J. Hazard. Mater. 248–249, 202–210. doi:10.1016/j.jhazmat.2013.01.012.

Williams, M.L., Carslaw, D.C., 2011. New directions: science and policy – out of step on NOx and NO_2? Atmos. Environ. 45, 3911–3912. doi:10.1016/j.atmosenv.2011.04.067.

Xia, S.J., Liu, F.X., Ni, Z.M., Xue, J.L., Qian, P.P., 2013. Layered double hydroxides as efficient photocatalysts for visible-light degradation of Rhodamine B. J. Colloid Interface Sci. 405, 195–200. doi:10.1016/j.jcis.2013.05.064.

Xu, S.M., Pan, T., Dou, Y.B., Yan, H., Zhang, S.T., Ning, F.Y., Shi, W.Y., Wei, M., 2015. Theoretical and experimental study on $M^{II}M^{III}$-layered double hydroxides as efficient photocatalysts toward oxygen evolution from water. J. Phys. Chem. C 119, 18823–18834. doi:10.1021/acs.jpcc.5b01819.

Yamada, H., Hayashi, R., Tonokura, K., 2016. Simultaneous measurements of on-road/in-vehicle nanoparticles and NOx while driving: actual situations, passenger exposure and secondary formations. Sci. Total Environ. 563–564, 944–955. doi:10.1016/j.scitotenv.2015.11.093.

Zhao, Y., Zhang, S., Li, B., Yan, H., He, S., Tian, L., Shi, W., Ma, J., Wei, M., Evans, D.G., Duan, X., 2011. A family of visible-light responsive photocatalysts obtained by dispersing CrO_6 octahedra into a hydrotalcite matrix. Chem. Eur. J. 17, 13175–13181. doi:10.1002/chem.201101874.

Zhao, Y., Li, B., Wang, Q., Gao, W., Wang, C.J., Wei, M., Evans, D.G., Duan, X., O'Hare, D., 2014. NiTi-layered double hydroxides nanosheets as efficient photocatalysts for oxygen evolution from water using visible light. Chem. Sci. 5, 951–958. doi:10.1039/C3SC52546E.

Zhao, Y., Jia, X., Waterhouse, G.I.N., Wu, L.Z., Tung, C.H., O'Hare, D., Zhang, T., 2016. Layered double hydroxide nanostructured photocatalysts for renewable energy production. Adv. Energy Mater. 6, 1–20. doi:10.1002/aenm.201501974.